

A Mathematical Model of Bird Collisions With Wind Turbine Rotors

V. A. Tucker

Department of Zoology,
Duke University,
Durham, NC 27708

When a bird flies through the disk swept out by the blades of a wind turbine rotor, the probability of collision depends on the motions and dimensions of the bird and the blades. The collision model in this paper predicts the probability for birds that glide upwind, downwind, and across the wind past simple one-dimensional blades represented by straight lines, and upwind and downwind past more realistic three-dimensional blades with chord and twist. Probabilities vary over the surface of the disk, and in most cases, the tip of the blade is less likely to collide with a bird than parts of the blade nearer the hub. The mean probability may be found by integration over the disk area. The collision model identifies the rotor characteristics that could be altered to make turbines safer for birds.

1 Introduction

Wind plants that convert kinetic energy of the wind to electrical energy now exist in significant numbers around the world (Lamarre, 1992; Weinberg and Ancona, 1994). These plants avoid some of the environmental problems of fossil or nuclear-fueled power plants, but have a problem of their own: the blades of wind turbine rotors extract energy from the air by sweeping areas occupied by flying birds. Collisions with birds—particularly with raptors such as Red-tailed hawks (*Buteo jamaicensis*) and Golden eagles (*Aquila chrysaetos*)—more often kill the bird than damage the rotor, and federal laws protect these birds. Operators of wind plants that kill birds are subject to criminal prosecution (Tarnkins, 1993; Walcott, 1995). Moreover, individuals concerned about birds, and organizations such as the National Audubon Society and the Sierra Club, have opposed development of wind power in some localities until avian fatalities can be mitigated (Ferguson, 1994; Beyea, 1995). Avian fatality is perceived by some to be the major environmental problem with wind power (Everett, 1993; Davidson, 1994).

What can be done to reduce the probability of collisions between birds and rotor blades? This study develops a collision model that is prerequisite to an answer. The model analyzes the motions and dimensions of both birds and propeller-type rotor blades, and predicts the probability of a collision when the bird flies through the area swept by the blades. Except for Manning's collision model (1983), which is much less complete than the one presented here, no theoretical analysis of bird-rotor collisions appears to have been published. The present collision model will be used in another study (Tucker, 1996) to design rotors that can generate the same amount of electrical energy as most turbines in use today, but theoretically will collide with an order of magnitude fewer birds while doing so.

2 Description of Turbines, Birds, and the Wind

The turbines in this study have three components: (1) a rotor (Fig. 1) of the propeller type—i.e., the rotor is similar to an aircraft propeller with three blades—mounted on a shaft with a horizontal axis, (2) a nacelle structure that supports the rotor shaft, and (3) a tower that supports the nacelle structure. The nacelle yaws around a vertical axis and keeps the rotor shaft

parallel to the wind direction. Additional information on wind turbines can be found in Spera (1994).

This paper describes rotor blades with the usual terms for aircraft wings. The root of the blade attaches to a hub on the rotor shaft, and the tip is the end opposite to the root. The blade length (R) is the length of a straight length line between the center of the hub and the blade tip. The blade chord (c) is the length of the chord line, which is perpendicular to the length line and connects the leading and trailing edges of a cross section of the blade. The chord decreases from root to tip in a tapered blade, and the angles between the chord lines change from root to tip in a twisted blade. The blade thickness is the maximum dimension of the blade measured perpendicular to the length line and the chord line.

A system of orthogonal left-handed coordinates (Fig. 1) locates the rotor and the bird in space. The x -axis is the horizontal axis of the rotor shaft, with the origin at the hub and x values that increase in the downwind direction. The y -axis also is horizontal, and the z -axis is vertical. When viewed from a negative point on the x -axis, y values increase toward the right, and the rotor blades rotate around the x -axis in a counterclockwise direction (Fig. 1). The length lines are perpendicular to the x -axis and sweep out the rotor disk of radius R in the yz -plane as they rotate.

The azimuth angle ψ is on the yz -plane and is the angle between the y -axis and a line that passes through the origin. ψ specifies a blade position when the line is a length line, and ψ changes at rate Ω as the blade rotates. ψ also may be a polar coordinate of a point when the line connects the point and the origin and is of length r , the other polar coordinate.

The theoretical blades are either three dimensional or one dimensional. Three-dimensional blades have length, chord, and twist, but no thickness. The length line is the leading edge of the blade, and the chord and the twist angle (β) between a chord line and the rotor disk both vary with r . Thus, a chord line projects out of the plane of the disk unless $\beta = 0$. Controls for the rotor can adjust the pitch of the blades by rotating a blade around its length line and adding a pitch angle to the twist angles of the chord lines.

One-dimensional blades have only length, and are equivalent to three-dimensional blades with chord lines of zero length.

A bird in the collision model glides on fixed wings. It is two dimensional and rectangular (Fig. 1), with the longer dimension being the wing span (b) and the other dimension being the body length from the tip of the beak to the tip of the tail. The corners of the rectangle are numbered 1 through 4, with corner

Contributed by the Solar Energy Division of THE AMERICAN SOCIETY OF MECHANICAL ENGINEERS for publication in the ASME JOURNAL OF SOLAR ENERGY ENGINEERING. Manuscript received by the ASME Solar Energy Division, Sept. 1995; final revision, Jan. 1996. Associate Technical Editor: P. S. Veers.

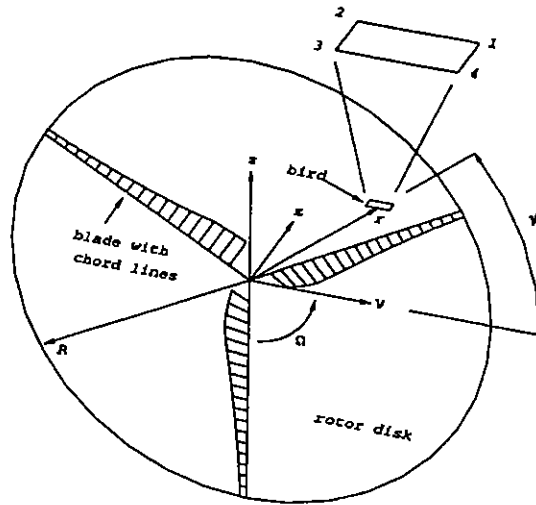


Fig. 1 A three-dimensional view of the model rotor and bird. The leading edges of the three-dimensional rotor blades sweep out the rotor disk of radius R as the blades rotate at angular speed Ω . The disk is in the yz -plane of the orthogonal coordinate system x, y, z ; and the polar coordinates r, ψ locate points on the disk—in this case, a point on the model bird (small rectangle parallel to the xy -plane). The bird has a wing span of $0.1 R$, which is a typical proportion for a rotor and a Red-tailed hawk. The enlarged rectangle shows the numbering system for the corners of the bird. The chord lines on the blades are at intervals of $0.05 R$.

1 at the right front from the bird's point of view, corner 2 at the left front and corner 4 at the right rear. The ratio of wing span to body length is the aspect ratio (A). The bird always occupies a plane that is parallel to the xy -plane, and the wing span may have any orientation in the plane.

The bird moves relative to the air with velocity V_b , and relative to the ground with velocity V :

$$V = V_b + (1 - a)U \quad (1)$$

where U is the wind velocity relative to the ground. Symbols in boldface the term "velocity" indicate vectors, in contrast to the term "speed," which is the magnitude of the vector. The coordinate system for V and U is the xyz system described previously, and the coordinate system for V_b is a parallel xyz system that moves with the wind. U is always parallel to the x -axis and directed toward increasing x values. Once specified, the variables in Eq. (1) are constant in the region swept by the rotor blades.

The quantity a in Eq. (1) is the axial induction factor (Wilson, 1994), and it accounts for the fact that air flowing through the disk has a speed less than U . The value of a is 0 far from the turbine, but a increases as air approaches the turbine and slows down. At the disk, a is one-third for a rotor that converts the maximum proportion of kinetic energy in the air to mechanical energy.

3 The Collision Model

A collision occurs when a bird and a rotor blade occupy the same region in space and time. The model does not distinguish different severities of collisions, and a collision may be a mere brush of a wing tip against a blade or a head-on contact.

The probability of a collision has a value between 0 and 1, and can be defined as a ratio of times. As the bird penetrates the rotor disk at some random point, it occupies a region where it may collide with a blade. The blade sweeps through this region in the time interval Δt_1 , and since the blade makes a complete revolution in time interval Δt_2 , the probability is proportional to $\Delta t_1 / \Delta t_2$. The mathematical equations for proba-

Nomenclature

A = aspect ratio of bird	V_{bx}, V_{by} = components of bird velocity relative to air (m/s)	Δy_b = dimension of bird parallel to y -axis (m)
a = axial induction factor	V_x, V_y = components of bird velocity relative to ground (m/s)	$\Delta\psi$ = change in azimuth angle (radians)
B = number of blades in rotor	v_0 = tangential threshold speed of blade (m/s)	$(\Delta\psi)_x$ = x -dependent range of ψ (radians)
b = wing span of bird (m)	w = component of downwash velocity (m/s)	$(\Delta\psi)_s$ = s -dependent range of ψ (radians)
k_1 = empirical constant (m)	x, y, z = spatial coordinates (m)	
k_2 = empirical constant		
c = chord of blade (m)	Vectors	Greek symbols
p = probability of collision	V = bird velocity relative to ground (m/s)	α = angle of attack of blade (radians)
p_{1D} = probability for one-dimensional blades	V_b = bird velocity relative to air (m/s)	α_R = angle of attack at the blade tip (radians)
p_a = probability due to active behavior	U = wind velocity relative to ground (m/s)	β = angle between a chord line of blade and the rotor disk (radians)
p_c = probability term for a three-dimensional blade		$\beta_0 = \beta$ when $s_1 = s_2$ (radians)
p_p = probability due to passive behavior	Delta quantities	β_i = angle between a chord line of the blade and the rotor disk when β at the blade tip is 0 (radians)
p_s = s -component of probability	Δr = change in radius (m)	π = ratio of circumference to diameter of a circle
p_x = x -component of probability	Δs = arc component (m)	ϕ = angle between relative wind and rotor disk (radians)
\bar{p} = mean probability	Δs_b = arc component of bird (m)	$\phi_R = \phi$ at the blade tip (radians)
R = radius of rotor disk (m)	Δs_c = arc component of the blade chord (m)	ψ = azimuth angle on rotor disk (radians)
r = radius (m)	Δt = time interval (s)	Ω = angular speed (radians/s)
r_0 = minimum radius (m)	Δx = x -component (m)	
s = arc length (m)	Δx_b = dimension of bird parallel to x -axis (m)	
s_1, s_2 = arc lengths for a three-dimensional blade (m)	Δx_c = dimension of rotor blade parallel to x -axis (m)	
t = time (s)	Δy = y -component (m)	
U = wind speed relative to ground (m/s)		
V = bird speed relative to ground (m/s)		
V_b = bird speed relative to air (m/s)		

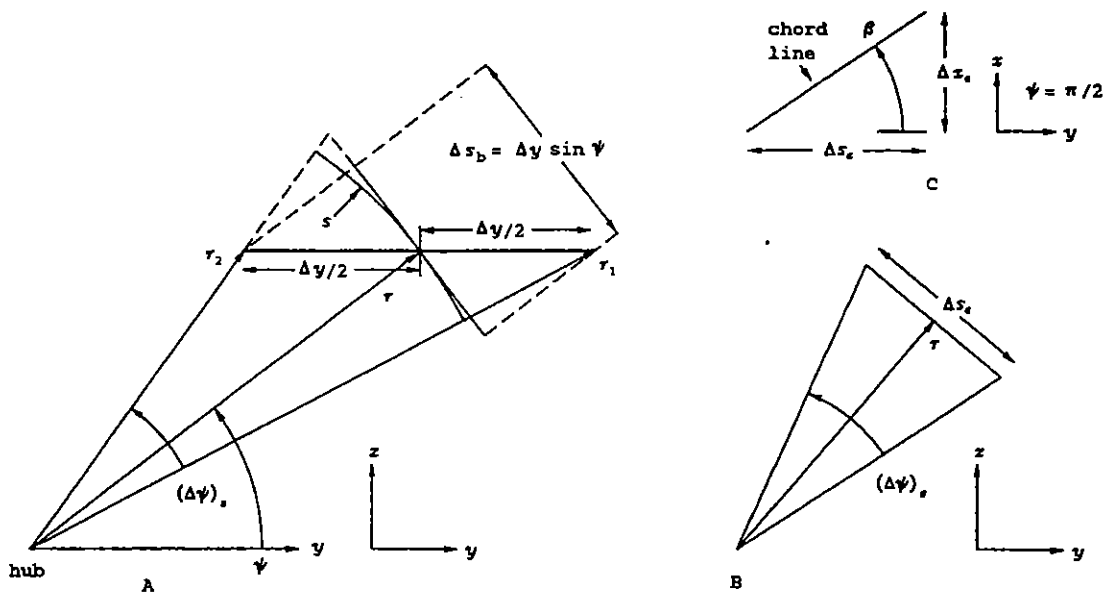


Fig. 2 Examples of x and s -components for a bird (A) and a three-dimensional blade (B, C). Each drawing is an orthogonal projection on a plane, and pairs of coordinates adjacent to the drawing identify the plane. Drawings A and B are projections on the yz -plane, and drawing C is a projection on the xy -plane. Drawing A shows a heavy horizontal line of length Δy that represents the bird's wing span. The line is at distance r from the rotor hub, and Δs_b and $(\Delta\psi)_a$ are the arc-component and the arc-dependent range of ψ , respectively, for the wing span. Drawing B shows the arc-component, Δs_c , of a three-dimensional blade, and the arc-dependent range of ψ , $(\Delta\psi)_a$, for the arc component. The arc-component is a projected chord line with a midpoint that is distance r from the origin. Drawing C shows the x -component, Δx_c , and the arc-component, Δs_c , of a chord line of a three-dimensional blade.

bility are simpler if the blade is regarded as the hand of a clock, and Δt_1 and Δt_2 are replaced by changes in the azimuth angle of the blade. The blade sweeps through the angle $\Delta\psi = \Omega\Delta t_1$ in time Δt_1 , and through the angle 2π in time Δt_2 .

The bird's behavior as it passes through the rotor influences Δt_1 , and hence the probability of a collision, p . This paper accounts for the behavior of the bird by defining p as the product of two factors:

$$p = p_p p_a \quad (2)$$

p_p is the probability of a collision when the bird behaves passively and does not change its shape or velocity in response to the rotor blades, whereas the value of p_a depends on the actions the bird takes to avoid the blades. For example, $p_a = 0$ for a hawk that perceives the moving blades and maneuvers between them as it passes through the disk; but $p_a = 1$ for a hawk that makes no attempt to avoid the blades, perhaps because it is intent on prey and not paying attention to the rotor.

p_a is 1 in the collision model, except at points on the disk within the minimum radius (described in Section 3.5) where p_a is 0. When p_a is 1, p is the product of the number of blades B and the ratio of the two angles mentioned above:

$$p = B\Delta\psi/(2\pi) \quad (3)$$

3.1 x and s -Components. The collision model finds $\Delta\psi$ from two spatial components: the x -component, Δx , and the s -component (or arc-component), Δs . These components exist for both the bird and a three-dimensional blade, but a one-dimensional blade lacks both components because it has no chord. The following sections describe these components for both the bird and a blade, with references to Fig. 2.

Δx determines the time, Δt , that the bird takes to pass through the disk and clear the blade:

$$\Delta t = \Delta x/|V_x| \quad (4)$$

where V_x is the component of the bird's ground velocity that is

parallel to the x -axis. A collision occurs when the blade in time Δt sweeps through a region that contains the bird.

Δs measures the length of an arc swept out by a point on the blade. A collision occurs if the point is on that arc when the bird enters the region swept by the blade.

To get an intuitive feel for the Δx and Δs -components, consider a one-dimensional spear thrown through a disk swept by one-dimensional blades. The spear is parallel to the x -axis so that Δx is the length of the spear and Δs is 0. The probability that a blade will cut the spear in the time that the spear takes to pass through the disk depends on Δx . Now consider the spear flung crossways through the disk and directly above the hub, so that the spear is horizontal and parallel to the disk. Δx is now zero and Δs , the length of the spear, approximates an arc at the radius where the spear penetrates the disk. The spear may still collide with a blade, but now with a probability that depends on Δs .

3.1.1 x and s -Components for the Bird. The x -component for the bird arises because the bird has a dimension Δx_b that is parallel to the x -axis, and the s -component arises because the bird also has a dimension Δy_b that is parallel to the y -axis. Since this study does not describe rotor blades in terms of a dimension parallel to the y -axis, the subscript may be dropped:

$$\Delta y = \Delta y_b \quad (5)$$

Δy gives rise to an arc component Δs_b that approximates an arc length (Fig. 2(a)) and is a function of ψ :

$$\Delta s_b = \Delta y \sin \psi \quad (6)$$

3.1.2 x and s -Components for Three-Dimensional Rotor Blades. These components arise because of the chord of the blades (Fig. 2B, 2C). For three-dimensional blades,

$$\Delta x_c = c \sin \beta \quad (7)$$

$$\Delta s_c = c \cos \beta \quad (8)$$

3.1.3 x and s -Components for the Combined Bird and Rotor Blade. Δx is a function of both Δx_b and Δx_c , and Δs is a function of both Δs_b and Δs_c . Both functions will be derived during the analysis of flight past three-dimensional blades.

3.2 x and s -Dependent Ranges of ψ . The x and s -components give rise to $(\Delta\psi)_x$ and $(\Delta\psi)_s$, the x and s -dependent ranges of ψ , respectively. The x -dependent range is related to Δx because $(\Delta\psi)_x$ is the product $\Omega\Delta t$, and from Eq. (4),

$$(\Delta\psi)_x = \Omega\Delta x / |V_x|. \quad (9)$$

The s -dependent range is related to Δs because

$$(\Delta\psi)_s = s/r, \quad (10)$$

where s is an arc length approximated by Δs . $\Delta\psi$ is a function (derived in later sections) of $(\Delta\psi)_x$ and $(\Delta\psi)_s$.

For example, consider a bird flying downwind and parallel to the x -axis. The component Δy equals the bird's wing span, and the bird will strike the length line of a one-dimensional blade at the instant of penetration if the blade is in the range $(\Delta\psi)_x$ (Fig. 2(a)). The s -component of the bird is the component of Δy normal to the length line at position ψ , and the blade has no s -component. Therefore, $\Delta s = \Delta s_b$, and

$$\Delta s = \Delta y \sin \psi, \quad (11)$$

which approximates the arc length for $(\Delta\psi)_s$ at r (Fig. 2(a)). Therefore,

$$(\Delta\psi)_s \approx \Delta s/r. \quad (12)$$

The exact value of $(\Delta\psi)_s$ is, from Fig. 2(a),

$$(\Delta\psi)_s = \arctan \left(\frac{r \sin \psi}{r \cos \psi - \Delta y/2} \right) - \arctan \left(\frac{r \sin \psi}{r \cos \psi + \Delta y/2} \right). \quad (13)$$

As another example, consider a three-dimensional blade with chord c and the s -component Δs_c from Eq. (8). The s -dependent range of ψ for the blade (Fig. 2(b)) is

$$(\Delta\psi)_s \approx \Delta s_c/r. \quad (14)$$

The combined s -component Δs for the bird and the blade together is a function (derived in later sections) of Δs_b and Δs_c , and

$$(\Delta\psi)_s \approx \Delta s/r. \quad (15)$$

3.3 Approximations. The approximation in Eq. (12) causes an error in p that depends on r and ψ , but the error is negligible in typical turbines in use today. For example, r_0 (Section 3.5) typically is greater than 3 m when v_0 is 25 m/s. If a bird with a wing span of 1 m passes through the rotor disk at points with radii of 3 m, the approximation causes an error in p of less than 0.015 for a rotor with three blades. The error decreases for smaller wing spans and larger radii.

The approximation in Eq. (14) causes an even smaller error in p : less than 1.2×10^{-4} for a three-bladed rotor.

The model ignores edge effects at the periphery of the disk where only part of the bird passes through the disk. In effect, a blade has an additional virtual length of up to half a wing span. This artefact is small, because most birds have wing spans less than 0.05 times the diameters of rotors in use today.

The model does not account for changes in chord and twist angle along short lengths, Δr , of a three-dimensional blade. For example, points 1 or 2 on the bird might strike the leading edge of the blade, but they usually do so at points Δr apart (Fig. 2(a)), where

$$\Delta r = r_1 - r_2. \quad (16)$$

The model uses constant values for the chord and the twist angle between r_1 and r_2 .

3.4 Probability Contour Maps and the Mean Probability of a Collision. The model describes the probability of a collision at each point (described by coordinates r, ψ) on the rotor disk. Probability contour maps show curves (or contours) on the disk that are loci of points for given probabilities of collisions. The mean probability, \bar{p} , of a collision is the spatial average of the probabilities over the surface of the disk:

$$\bar{p} = \frac{2}{\pi(R^2 - r_0^2)} \int_0^\pi \int_{r_0}^R p r dr d\psi. \quad (17)$$

The value of the double integral can be thought of as the volume of a solid whose base is half of a disk with a hole of radius r_0 at the center. The height of the solid above any point on the base is the probability of a collision at that point. The mean probability of collision is the volume of the solid divided by the area of the base.

3.5 r_0 , the Minimum Radius for \bar{p} . The lower limit r_0 of the inner integral in Eq. (17) is the minimum radius at which model birds collide with a rotor blade—i.e., $p_a = 0$ for points on the blades with radii less than r_0 , and $p_a = 1$ at larger radii. r_0 is inversely proportional to Ω , because a model bird does not collide with points on the blade with tangential speeds less than the constant v_0 , the tangential threshold speed:

$$r_0 = v_0/\Omega. \quad (18)$$

This characteristic of the model bird is meant to represent the behavior of real birds, which are able to avoid collisions by flying around slow-moving objects, such as the blades near the rotor hub.

3.6 Downwind, Upwind, and Crosswind Flight. The remainder of this paper analyzes the probability of a collision under several circumstances: when the bird passes downwind, upwind, or across the wind through a rotor with one dimensional blades; and downwind or upwind through a rotor with three-dimensional blades. In each case, $(\Delta\psi)_x$ and $(\Delta\psi)_s$ are expressed in terms of V_x , Δx and Δs ; and then $\Delta\psi$ is expressed in terms of $(\Delta\psi)_x$ and $(\Delta\psi)_s$. Given $\Delta\psi$, Eq. (3) yields the probability of a collision at each point on the rotor disk.

4 One-Dimensional Blades and Flight Parallel to Wind Direction

This section analyzes the simplest interaction between the bird and the rotor: the bird glides parallel to the wind direction and through a rotor with one-dimensional blades. Points 1 and 2 on the bird penetrate the disk at time t , and points 3 and 4 penetrate at time $t + \Delta t$ (Fig. 3). The interval Δt is given by Eq. (4).

4.1 Analysis. The x -component Δx equals Δx_b , the distance between points 1 and 4 on the bird, since Δx_c is 0 for a one-dimensional blade. Δx depends on the bird's wing span, b , and aspect ratio, A :

$$\Delta x = b/A. \quad (19)$$

For flight parallel to the wind direction, the bird's ground and air velocities have only the x -components V_x and V_{bx} , respectively, and

$$V_x = V_{bx} + (1 - a)U. \quad (20)$$

V_x is positive for downwind flight, and both V_x and V_{bx} are negative for upwind flight.

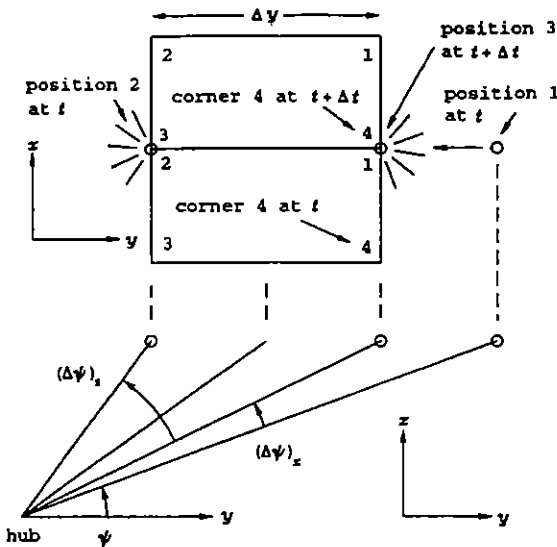


Fig. 3 The range of positions that a one-dimensional blade must occupy to strike a bird that passes through the rotor disk in a direction parallel to the wind. The top part of the figure is a projection on the xy -plane, and the bottom part is a projection on the yz -plane (pairs of coordinates adjacent to each part identify these planes). The top part of the figure shows the bird projected on the xy -plane at two different times, and circles mark positions where blades intersect the plane occupied by the bird. Bursts of radiating lines around two of the circles indicate that the bird collides with blades at those positions at the indicated times. The bottom part of the figure shows the same blade positions indicated in the top part, but in the yz -plane. A blade at position 1 (rightmost) at time t moves to position 3 at time $t + \Delta t$. During this time interval, corner 4 of the bird moves toward the rotor disk; and the blade strikes corner 4 at position 3. A blade at position 2 (leftmost) is struck by corner 2 of the bird at time t . Blade positions 1 and 3 bound the x -dependent range of ψ , $(\Delta\psi)_x$; and positions 2 and 3 bound the s -dependent range of ψ , $(\Delta\psi)_s$. Positions 1 and 2 bound $\Delta\psi$, the sum of $(\Delta\psi)_x$ and $(\Delta\psi)_s$.

The s -component, Δs , equals Δs_b , since Δs_c is 0 for a one-dimensional blade. $\Delta y = b$, and from Eq. (6),

$$\Delta s = b \sin \psi. \quad (21)$$

Figure 3 shows the range of positions that a rotor blade must occupy for a collision to occur. Since $(\Delta\psi)_x$ and $(\Delta\psi)_s$ are contiguous but nonoverlapping,

$$\Delta\psi = (\Delta\psi)_x + (\Delta\psi)_s. \quad (22)$$

4.2 Probability and Mean Probability of a Collision. The probability of collision during flight parallel to the wind direction is found by combining Eq. (22) and (3) after substituting expressions for V_x , Δx , and Δs into Eq. (9) and (12) to find $(\Delta\psi)_x$ and $(\Delta\psi)_s$:

$$p = \frac{Bb}{2\pi} \left(\frac{\Omega}{A|V_{bx} + (1-a)U|} + \frac{\sin \psi}{r} \right). \quad (23)$$

The probability contours (for example, see Section 7.1) for this equation are circles tangent to the origin, because r is proportional to $\sin \psi$ when p and other variables are constant.

The mean probability of a collision for birds passing through the disk at random points may now be calculated with Eq. (17). After integration,

$$\bar{p} = \frac{Bb}{2\pi} \left(\frac{\Omega}{A|v_{bx} + (1-a)U|} + \frac{4}{\pi \left(R + \frac{v_0}{\Omega} \right)} \right). \quad (24)$$

Equations (23) and (24) describe both downwind flight ($V_{bx} > 0$) and upwind flight ($V_{bx} + (1-a)U < 0$).

5 One-Dimensional Blades and Flight Oblique to Wind Direction

This section analyzes the interaction between a one-dimensional turbine blade and a bird flying through the rotor disk in an oblique direction; i.e., not parallel to the wind direction. The analysis has more variables than that for parallel flight, because the bird's velocity relative to the ground now has two components: V_x perpendicular to the rotor disk and V_y parallel to it. In addition, the orientation of the bird relative to the disk becomes a variable; i.e., points 1 and 2 on the bird no longer penetrate the disk at the same time. Finally, for a given ground velocity V , the component V_y and the horizontal component of the blade's tangential velocity change directions relative to one another, depending on whether the point of penetration is above or below the hub. This situation arises because the blade's tangential velocity component has opposite directions above and below the hub.

5.1 Analysis. When penetration is above the hub and V_y is positive, the blade approaches the front of the bird and may strike the bird's leading edge (the line between points 1 and 2). When V_y is negative, the blade follows the bird; i.e., V_y has the same direction as the horizontal component of the blade's tangential velocity. Over most of the disk area, the following blade may overtake the bird from behind and strike its trailing edge (the line between points 3 and 4). In a small region, most of which is near the center of the disk, the bird may overtake the blade and strike the blade's trailing edge.

When penetration is below the hub, the situation is as described above, but with a reversed sign for the tangential velocity component.

To simplify the analysis, this section considers oblique flight during which the bird penetrates the disk above the hub with two restrictions: (1) The bird's air velocity is perpendicular to the wind direction so that V_{bx} is 0, and $|V_{by}|$ is the bird's air speed. In this case, the wing span is perpendicular to the rotor disk, and points 2 and 3 on the bird penetrate the disk simultaneously. (2) No collisions occur in the region of the disk where the bird may overtake the blade. All but a trivial part of this region ordinarily is inside the minimum radius r_0 .

With these restrictions, the x -component equals the bird's wing span,

$$\Delta x = b, \quad (25)$$

the time interval, Δt , for the bird to pass through the disk is given by Eq. (4) and the ground velocity component, V_x , (from Eq. (1)) is

$$V_x = (1-a)U. \quad (26)$$

The s -component, Δs , equals Δs_b , since Δs_c is 0 for a one-dimensional blade. Δs arises from two displacements along the y -axis (Fig. 4): the body length, b/A , of the bird, and the translation of the bird for distance $V_{by}\Delta t$ along the y -axis. Combining these, the s -component is

$$\Delta s = (b/A + V_{by}\Delta t) \sin \psi. \quad (27)$$

This equation describes both approaching and following blades, depending on whether V_{by} is positive or negative. Since $(\Delta\psi)_x$ and $(\Delta\psi)_s$ are contiguous,

$$\Delta\psi = (\Delta\psi)_x + (\Delta\psi)_s, \quad (28)$$

as was the case for flight parallel to the wind.

5.2 Probability and Mean Probability of a Collision. The probability of collision, from Eq. (28) and (3) with expressions for V_x , Δx and Δs substituted into Eq. (9) and (12), is

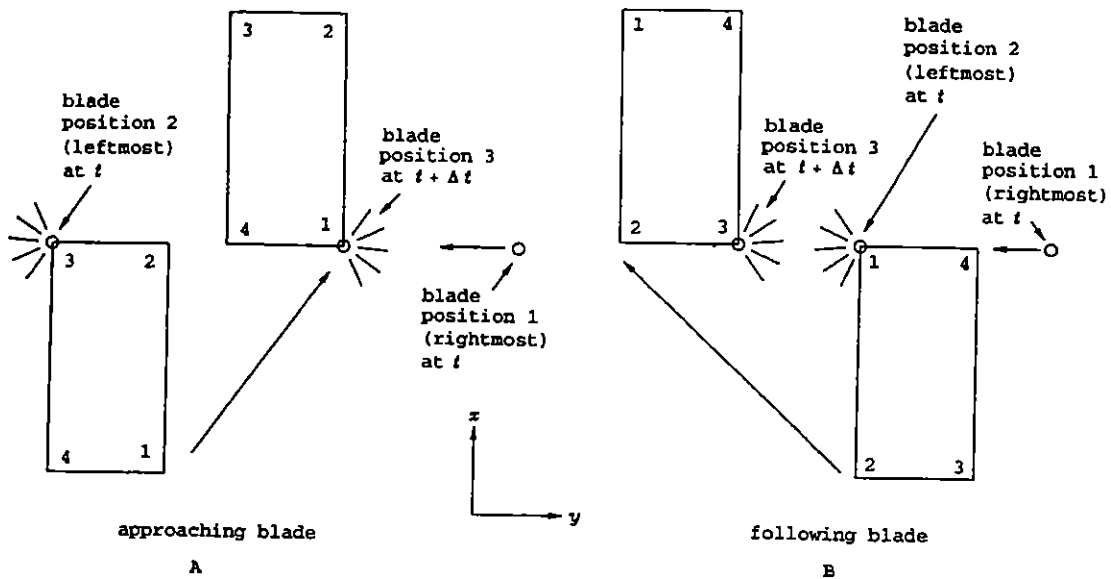


Fig. 4 A bird passing through the rotor disk as it flies across the wind. The drawing orientation and conventions are the same as those in the top part of Fig. 3. In drawing A, an approaching blade strikes the bird moving to the right; and in drawing B, a following blade strikes the bird moving to the left. In both cases, the blade is one-dimensional and moves from right to left. In drawing A, a collision occurs if the blade is anywhere between a rightmost position (position 1) and a leftmost position (position 2). A blade at position 1 at time t moves to position 3 at time $t + \Delta t$. During this time interval, corner 1 of the bird moves to the right and toward the rotor disk to a point where it is struck by the approaching blade at position 3. A blade at position 2 is struck by corner 3 of the bird at time t . In drawing B, a collision occurs if the blade is anywhere between a rightmost position (position 1) and a leftmost position (position 2). A blade at position 1 moves to position 3 at time $t + \Delta t$. During this time interval, corner 3 of the bird moves to the left and toward the rotor disk to a point where it is struck by the following blade at position 3. A blade at position 2 is struck by corner 1 of the bird at time t .

$$p = \frac{Bb}{2\pi} \left(\frac{\Omega}{(1-a)U} + \frac{\sin \psi}{r} \left(\frac{1}{A} + \frac{V_{by}}{(1-a)U} \right) \right) \quad (29)$$

The mean probability of a collision now may be calculated with Eq. (17). After integration,

$$\bar{p} = \frac{Bb}{2\pi} \left(\frac{\Omega}{(1-a)U} + \frac{4 \left(\frac{1}{A} + \frac{V_{by}}{(1-a)U} \right)}{\pi \left(R + \frac{v_0}{\Omega} \right)} \right) \quad (30)$$

Equations (29) and (30) describe both advancing and following blades, depending on whether V_{by} is positive or negative, respectively.

The probability contours (for example, see Section 7.1) for approaching blades, like those for parallel flight, are circles tangent to the origin because r is proportional to $\sin \psi$ for a given probability. The contours for following blades ($V_{by} < 0$) also are circles, with one exception. If $1/A = -V_{by}/V_x$, then the second term in Eq. (29) disappears (see Eq. (26)), and the probability of a collision is the same at all points on the semi-disk. Otherwise, if $1/A < V_{by}/V_x$, the probability of collisions decreases from the periphery of the semi-disk towards the center. If $1/A > V_{by}/V_x$, the probability of collisions increases from the periphery toward the center.

To get an intuitive feel for these changes in probability when $V_{by} < 0$, consider a bird described by Eq. (29) when $V_{by} = 0$ and all other variables are constant. The bird is stationary relative the air but moves through the rotor disk at the wind velocity. The probability of a collision is higher near the center of the disk than at the periphery, because the analysis of the situation is the same as that in the previous section for a bird moving parallel to the wind direction. Now, if the bird begins to fly with $V_{by} < 0$, the probability at a given point decreases because the blades are following the bird, and the closing speed between

them and the bird is less than it was when $V_{by} = 0$. The decrease is greater at the smaller values of r near the center of the disk, thereby reducing the disparity in the probabilities near the center and at the periphery.

If $V_{by} = -V_x/A$, the probabilities become equal; and if V_{by} becomes even more negative, the probabilities become lower near the center of the disk than at the periphery.

6 Three-Dimensional Blades and Flight Parallel to Wind Direction

This section analyzes the interactions between a bird and a three-dimensional rotor blade. The bird flies through the rotor disk in directions parallel to the wind direction, both downwind and upwind.

6.1 Analysis of Downwind Flight.

6.1.1 Types of Collisions. The bird glides downwind ($V_y = 0$ and $V_{bx} > 0$) through the rotor with a positive ground velocity component, V_x , given by Eq. (20), and may collide with the leading edge of a blade, or with some part of the chord line between the leading and trailing edges. The analysis for leading edge collisions is identical to that for one-dimensional blades, since the leading edge is the length line. The analysis below for collisions with the chord line accounts for the chord and the twist angle of the three-dimensional blade.

A collision with the chord line may occur in one of two ways (Fig. 5). In a type 1 collision, the leading edge of the blade moves away from the bird, but point 2 on the bird strikes the chord line before the blade moves out of range. In a type 2 collision, the leading edge of the blade approaches the bird, and the chord line strikes the bird at point 4.

One or the other of the two types of collisions occurs when the blade is between positions 1 and 2 at time t (Fig. 5). As the blade moves from position 1 to 2, a point on the blade at radius r sweeps out an arc, the length of which depends on the

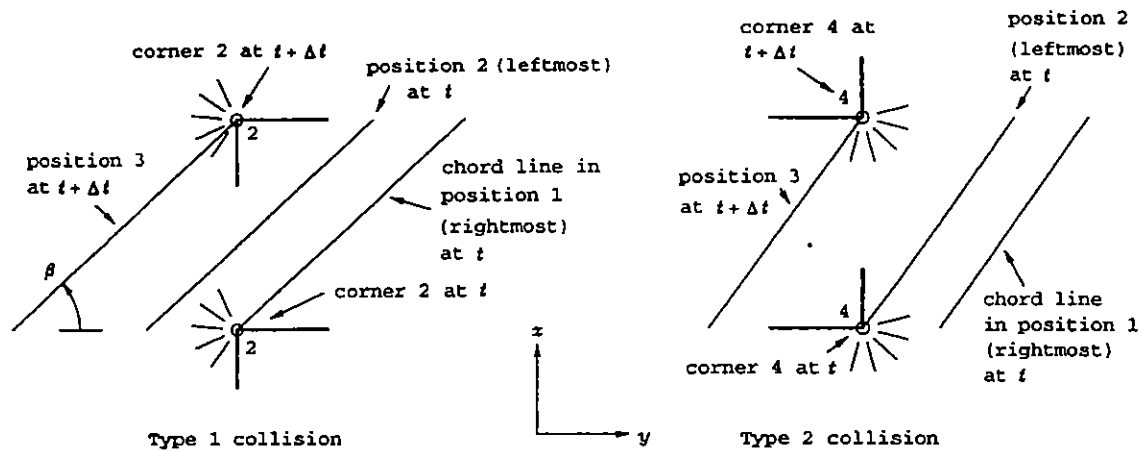


Fig. 5 Type 1 and type 2 collisions (see text) between a bird (only corners 2 or 4 are shown, in dark lines) and the chord line of a three-dimensional blade during downwind flight. The drawing orientation and conventions are the same as those in the top part of Fig. 3, and the chord line projections are shown when $\psi = \pi/2$. Type 1 collisions can occur between corner 2 of the bird and the blade when the chord line has a certain range of twist angles (see text), and the blade is anywhere between a rightmost position (position 1) and a leftmost position (position 2). A blade at the rightmost position at time t is struck by corner 2 of the bird. A blade at the leftmost position moves to position 3 at time $t + \Delta t$. During this time interval, corner 2 moves forward and strikes the blade at position 3. Between positions 1 and 3, a point on the blade moves through arc length s_1 (see text). Between positions 2 and 3, it moves through arc length s_2 . The arc length between positions 1 and 2 is $s_1 - s_2$. Type 2 collisions can occur between corner 4 of the bird and the blade when the chord line has a different range of twist from that for type 1 collisions (see text), and the blade is anywhere between a rightmost position (position 1) and a leftmost position (position 2). A blade at the rightmost position at time t moves to position 3 at time $t + \Delta t$. During this time interval, corner 4 moves forward and it is struck by the blade at position 3. A blade at the leftmost position strikes corner 4 at time t . Between positions 1 and 3, a point on the blade moves through arc length s_2 . Between positions 2 and 3, it moves through arc length s_1 . The arc length between positions 1 and 2 is $s_2 - s_1$.

x -component (Δx_c) and the s -component (Δs_c) of the blade. These components are related to the chord, c , and the twist angle, β , of the blade. Repeating Eq. (7) and (8),

$$\Delta x_c = c \sin \beta,$$

$$\Delta s_c = c \cos \beta.$$

The arc lengths associated with these two components are

$$s_1 \approx \Delta s_c, \quad (31)$$

and

$$s_2 = \Omega r \Delta x_c / V_x. \quad (32)$$

A type 1 collision occurs (Fig. 5) when the point on the blade sweeps through the arc length $s_1 - s_2$, provided that this length is positive. A type 2 collision occurs when the blade sweeps through the arc length $s_2 - s_1$, again provided that this length is positive. Since the two lengths have opposite signs, either a type 1 or a type 2 collision may occur, but not both.

Neither type of collision occurs when the arc length is 0. This situation arises when $c = 0$ or when $s_2 = s_1$. In the latter case, the motion of any point on the bird, relative to the blade, is parallel to the chord line, because, from Eq. (31) and (32),

$$\Omega r \sin \beta_0 / V_x = \cos \beta_0, \quad (33)$$

and

$$\beta_0 = \arctan \left(\frac{V_{bx} + (1-a)U}{\Omega r} \right). \quad (34)$$

A chord line with angle β_0 is parallel to the vector difference between the bird's velocity relative to the ground during downwind flight and the tangential velocity of a point on the blade at the radius where the bird penetrates the disk.

To get an intuitive feel for type 1 and 2 collisions, consider the approximate relative motion between a bird flying downwind and a rotor blade when the bird is about to penetrate the disk at a point r_1 , ψ_1 , and $\psi_1 = \pi/2$. The blade is approaching

ψ_1 , and r_1 is large. From the point of view of the bird, a point at r_1 on the leading edge of the blade is moving toward the bird and from the right along a path inclined at angle β_0 (from Eq. (34)) to the disk. Assume that the chord line at r_1 has the twist angle β_0 . In the bird's frame of reference, the chord line falls on the path followed by the point on the leading edge. If point 4 on the bird passes just to the left of the leading edge as the bird penetrates the disk, point 4 will remain just to the left of the chord line until point 4 passes the trailing edge. Thus, the bird cannot collide with the chord line, although it may collide with the leading edge with a probability given by Eq. (23) for one-dimensional blades.

Now assume that the chord line has an angle greater than β_0 . A type 2 collision occurs when point 4 passes just to the left of the leading edge, because point 4 will collide with the chord line before passing the trailing edge.

If the chord line has an angle less than β_0 , a type 1 collision can occur between point 2 on the bird and the chord line. Assume that point 2 passes just to the right of the leading edge as the bird penetrates the disk. Then point 2 will collide with the chord line before passing the trailing edge.

When the blade operates in a normal manner, only type 1 collisions may occur, because the chord line must have an appropriate angle of attack, α , between itself and the wind velocity vector relative to the blade. This angle of attack allows the blade section at the chord line to produce an aerodynamic force that turns the rotor, and it also causes β for the chord line to be less than β_0 . As a result, $s_1 - s_2$ is positive, and type 2 collisions cannot occur. The following equations provide details.

The angle, ϕ , between the wind velocity relative to the blade and the rotor disk,

$$\phi = \arctan \left(\frac{(1-a)U - w}{\Omega r} \right), \quad (35)$$

is less than β_0 because, compared to Eq. (34), V_{bx} is missing and w is positive. w is a component of downwash, an air flow induced by a blade that produces lift. The value of β ,

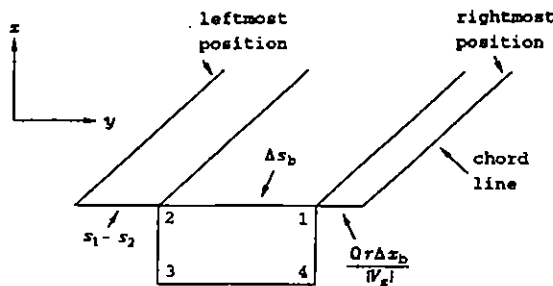


Fig. 6 The region that a three-dimensional blade must occupy between rightmost and leftmost positions to strike a bird that passes downwind through the rotor disk. The bird moves downwind (in the direction of increasing x), and parallel to the wind direction; and the chord lines move from right to left. The drawing orientation is the same as that in the top part of Fig. 3. The figure shows three parts of a projected arc, lined up with the leading edge of the bird. A point on the blade sweeps out the arc when the blade moves from the rightmost to the leftmost position, and $\psi \approx \pi/2$. The projected arc length $s_1 - s_2$ arises because of the chord of the three-dimensional blade (see Fig. 5), and the other two projections are identical to those for a one-dimensional blade. For clarity, the chord lines are disproportionately long, relative to the size of the bird.

$$\beta = \phi - \alpha, \quad (36)$$

is further reduced below β_0 because α normally is positive. Henceforth, I shall ignore type 2 collisions.

6.1.2 Probability of a Collision. This section describes collisions that occur between the bird and both the leading edge and the chord line of the blade. The total arc length, s , that the point on the blade must sweep out for a collision to occur may be read from Fig. 6:

$$s \approx \Omega r \Delta x_b / V_x + \Delta s_b + s_1 - s_2. \quad (37)$$

After substituting Eq. (31) and (32) and rearranging,

$$s \approx \frac{\Omega r (\Delta x_b - \Delta x_c)}{V_x} + \Delta s_b + \Delta s_c, \quad (38)$$

$$\Delta \psi = s/r \approx \frac{\Omega (\Delta x_b - \Delta x_c)}{V_x} + \frac{(\Delta s_b + \Delta s_c)}{r}. \quad (39)$$

Comparison of this equation with Eq. (9) and (10) shows that

$$\Delta x = \Delta x_b - \Delta x_c, \quad (40)$$

$$\Delta s = \Delta s_b + \Delta s_c, \quad (41)$$

and

$$\Delta \psi = (\Delta \psi)_x + (\Delta \psi)_s. \quad (42)$$

The probability of a downwind collision may now be found by combining Eq. (42) and (3) after substituting expressions for V_x , Δx and Δs into Eq. (9) and (12):

$$p = p_{1D} + p_c, \quad (43)$$

where p_{1D} is the probability in parallel flight of collisions with a one-dimensional blade (Eq. (23)), and

$$p_c = \frac{Bc}{2\pi} \left(\frac{\cos \beta}{r} - \frac{\Omega \sin \beta}{V_{bx} + (1-a)U} \right). \quad (44)$$

The term p_c accounts for the chord, c , and twist angle, β , of the three-dimensional blade. When c is 0, so is p_c , and Eq. (43) for a three-dimensional blade becomes the equation for a one-dimensional blade. The quantities c and β are functions of r given by the manufacturer's specifications for the blade.

The probability contours (for example, see Section 7.1) for collisions between the bird and a rotor with three-dimensional

blades are no longer circles, as they were for one-dimensional blades, because of the extra term p_c . (Calculation of contour lines for a given Ω can be simplified in some cases without appreciable error by an approximation for p_c :

$$p_c \approx k_1/r + k_2, \quad (45)$$

where k_1 and k_2 are the slope and intercept of a straight line fitted to the relation between p_c and $1/r$.)

6.1.3 Mean Probability of a Collision. The mean probability of a collision may be found with Eq. (17). After integration,

$$\bar{p} = \bar{p}_{1D} + \frac{B}{\pi(R^2 - r_0^2)} \times \int_{r_0}^R c \left(\cos \beta - \frac{r \Omega \sin \beta}{V_{bx} + (1-a)U} \right) dr \quad (46)$$

where \bar{p}_{1D} is the mean probability in parallel flight of a collision with a rotor with one-dimensional blades (Eq. (24)). (In some cases, the remaining integration in Eq. (46) can be simplified by using the approximation in Eq. (45).)

6.2 Analysis of Upwind Flight

6.2.1 Types of Collisions. When the bird flies upwind, both V_{bx} and V_x are negative. As with downwind flight, the bird may collide with the edge of a blade or with the chord line

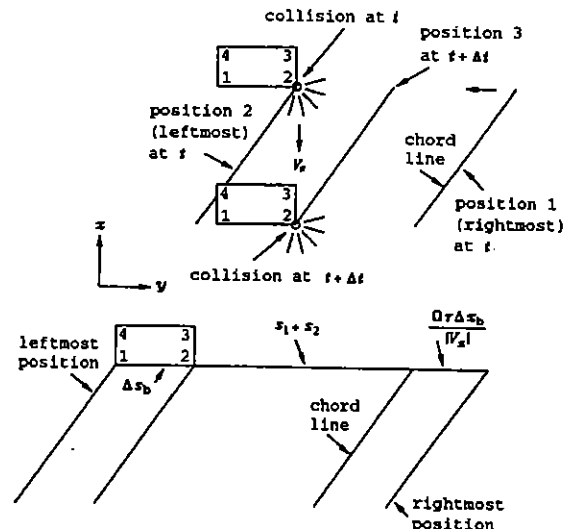


Fig. 7 (Top): Collisions between a bird and the chord line of a three-dimensional blade during upwind flight. The drawing orientation and conventions are the same as those in the top part of Fig. 3. The chord line projections are shown when $\psi = \pi/2$. A collision occurs between the left side of the bird (the line between corners 2 and 3) and the chord line if the blade is anywhere between a rightmost position (position 1) and a leftmost position (position 2). A blade at the rightmost position moves to position 3 at time $t + \Delta t$. During this time interval, corner 2 moves upwind to a point where it is struck by the blade at position 3, whereas a blade at the leftmost position strikes corner 2 at time t . The arc length between positions 1 and 2 can be found from arc lengths s_1 and s_2 , which are related, respectively, to the s and x -components for the blade (see text). Between positions 1 and 3, a point on the blade moves through arc length s_2 . Between positions 2 and 3, it moves through arc length s_1 . The arc length between positions 1 and 2 is $s_1 + s_2$. (Bottom): The region that a three-dimensional blade must occupy between rightmost and leftmost positions to strike a bird that passes upwind through the rotor disk. The drawing orientation and conventions are the same as those in Fig. 6. The projected arc length $s_1 + s_2$ arises because of the chord of the three-dimensional blade, and the other two projections are identical to those for a one-dimensional blade. For clarity, the chord lines are disproportionately long, relative to the size of the bird.

Table 1 Characteristics of the bird, the rotor, and the velocities used for the examples in Fig. 8 and Tables 2 and 3

Bird
 $b = 1 \text{ m}$, $A = 2$, $v_0 = 25 \text{ m/s}$

Rotor
 $B = 3$, $R = 10 \text{ m}$, $\Omega = 7.54 \text{ radians/s}$, $a = 0.25$

Chord of three-dimensional blade
 for r/R less than 0.1, $c/R = 0$
 from $r/R = 0.1$ to 0.25, $c/R = 0.115$
 from $r/R = 0.25$ to 1, $c/R = 0.168 - 0.240 r/R + 0.10 (r/R)^2$

Twist (in radians) of the chord lines along a three-dimensional blade
 (see text for additional explanation).

$$\beta_i = 0.640 \arctan \left(\frac{1}{8 \left(\frac{r}{R} - 0.015 \right)} \right) - 0.073$$

Velocity components (m/s) for the bird and the wind

Components	Downwind	Crosswind		Upwind
		blade: advancing following		
V_{bx} , V_{by}	5, 0	0, 5	0, -5	-10, 0
U	10	10	10	5

somewhere between the leading and trailing edges. The analysis for edge collisions is identical to the analysis for one-dimensional blades, since the edges are lines. The analysis below for chord line collisions accounts for the chord and the twist angle of the three-dimensional blade.

In contrast to downwind flight, a collision between the bird and the chord line can occur in only one way: point 2 on the bird may collide with the chord line (Fig. 7). For a collision to occur, the blade must be between positions 1 and 2 at time t . The approximate length of the arc swept out by a point at radius r on the blade as the blade moves from position 1 to 2 depends on the x and s -components (Eq. (7) and (8)) of the blade and the arc components s_1 and s_2 (Eq. (31) and (32)). A collision with the chord line occurs when the blade sweeps through the approximate arc length $s_1 + s_2$ (Fig. 7). Additional arc components, identical to those for a one-dimensional blade, arise because the bird may collide with the leading or trailing edge of the blade.

6.2.2 Probability and Mean Probability of a Collision. When the ground velocity component, $V_{bx} + (1 - a)U$, has the appropriate sign, Eqs. (43) through (46) describe both upwind and downwind flight.

7 Examples

The examples below were calculated from the collision model when the bird, the rotor and the wind have the characteristics listed in Table 1. The equation in this table for β_i , the twist of the chord lines, is an empirical equation for an existing rotor blade when the chord line at the blade tip is parallel to the rotor disk. In the examples, the collision model adjusts the pitch of three-dimensional blades so that β for each chord line equals β_i plus a constant that depends upon wind speed. The model keeps the angle of attack, α_R , of the blade tips at 0.0524 radians (3 deg), where α_R is the angle between the chord line and the direction, ϕ_R , of the relative wind at the tips. ϕ_R is given by Eq. (35) with $r = R$, and $w = 0$. Thus, pitch control sets β to $\beta_i + \phi_R - \alpha_R$.

7.1 Probability Contour Maps. Figure 8 shows the circular contours and probability values for downwind flight through a rotor with one-dimensional blades. Upwind and crosswind flight also have circular contours for rotors with one-dimensional blades. The reader can get an impression of the contour maps for flight in these other directions by using the probability values for two contour lines (Table 2): the contour line that forms the diameter when $\psi = 0$ or π , and the contour line that passes through the point $r = R/2$, $\psi = \pi/2$.

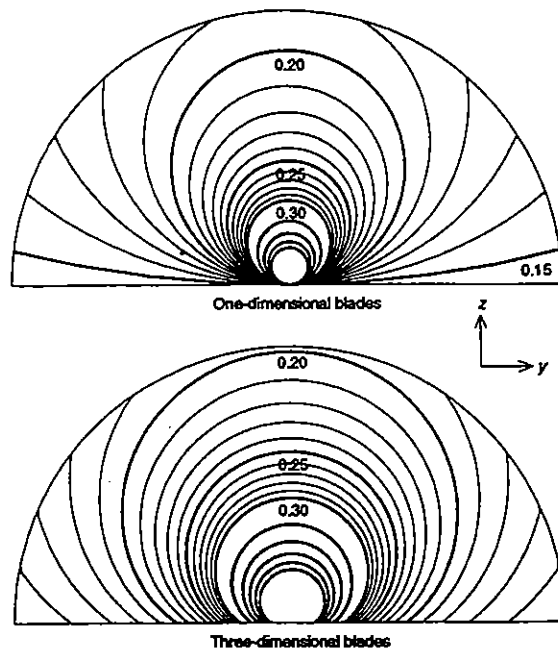


Fig. 8 Probability contour maps for downwind and upwind flight through a rotor with one-dimensional blades (top) and three-dimensional blades (bottom). Table 1 describes the bird and the rotor, and the numbers near the thick contours are the probabilities of collision. For probabilities greater than 0.30, only thick contours are shown, without probability values. None of the contours on either drawing represent the minimum radius, r_0 .

(Top): Circular probability contours for downwind flight through a rotor with one-dimensional blades. Contours for upwind and crosswind flight are also circular, and the contour values for these directions may be estimated from data in Table 2.

(Bottom): Distorted circular probability contours for downwind flight through a rotor with three-dimensional blades. Table 1 describes the bird and the rotor, and the numbers on the contours are the probabilities of collision. Contours for upwind flight are also distorted circles.

Figure 8 also shows the distorted circular contours typical of three-dimensional blades. The probability values in the figure describe downwind flight.

Surprisingly, the fast-moving tip of the blade in most cases is the least likely part of the rotor to be involved in a passive collision at a given value of ψ . The greater the distance from the hub, the greater the distance between the blades; and a bird has a greater chance of passing between them unscathed. The exception is crosswind flight with following blades, in which case the probability of a collision may be higher at the tip of the blade than near the center of the disk (see Section 5.2).

For flight parallel to the wind, the safest regions are where the wing span is parallel to the length lines; i.e., when $\psi = 0$ or π . The more dangerous regions are where the full span of

Table 2 The probability of a collision, p , between a bird and a one-dimensional blade along a diameter of the rotor disk ($\psi = 0$ or π) and at a point on the disk ($\psi = \pi/2$, $r = R/2$). See Section 7.2 for an explanation of the components p_x and p_y .

Flight direction	p at $\psi = 0$ or π ($p = p_x$)	p at $\psi = \pi/2$, $r = R/2$	p_x at $\psi = \pi/2$, $r = R/2$
Downwind	0.144	0.239	0.095
Upwind	0.288	0.383	0.095
Crosswind			
Advancing blades	0.480	0.591	0.111
Following blades	0.480	0.464	-0.016

Table 3 The mean probability of a collision between a bird and one and three-dimensional rotor blades

Flight direction	One-dimensional blades	Three-dimensional blades
Downwind	0.191	0.217
Upwind	0.335	0.397
Crosswind		
Advancing blades	0.535	—
Following blades	0.472	—

the wings must pass through shorter distances between the blades; i.e., near the hub when $\psi = \pi/2$ or $3\pi/2$.

7.2 Components of Probabilities. The probability of a collision at each point on the rotor disk can be broken down into an x -component, p_x , and an s -component, p_s , related to the time and space that the bird takes to pass through the disk. Combining Eq. (3) and Eq. (22):

$$p_x = B(\Delta\psi)_x / (2\pi), \quad (47)$$

$$p_s = B(\Delta\psi)_s / (2\pi), \quad (48)$$

and the probability is the sum of these components:

$$p = p_x + p_s. \quad (49)$$

For rotors with one-dimensional blades, p_x is constant at all points on the rotor disk, but p_s varies from point to point. $p_x = p$ at points on the horizontal diameter of the rotor, since $p_s = 0$ when $\psi = 0$ or π . Table 2 shows p_x values, and p_s values at the point $r = R/2$, $\psi = \pi/2$, for flights in various directions. p_s is $\frac{2}{3}$ or less of p_x in these examples, and even may be negative for crosswind flight with following blades.

7.3 Mean Probabilities. Table 3 shows the mean probabilities of collision, averaged over the rotor disk, of flights in different directions. Downwind flight is the safest. Upwind flight is not directly comparable with downwind and crosswind flight in these examples, because the values of V_{br} and U have been changed to make the ground velocity component V_x negative. Clearly, upwind flight through a rotor is an exceedingly risky maneuver for a bird, because p increases as V decreases; and V can approach 0 during upwind flight in windy conditions. In fact, $p = 1$ before V reaches 0 because birds have a nonzero dimension parallel to the x -axis. Crosswind flight is also risky

because, compared to downwind flight, a longer dimension of the bird passes through the disk at a slower speed.

Table 3 also shows the effect on mean probabilities of using the more complex model for three-dimensional blades rather than the simpler model for one-dimensional blades. During downwind flight, the mean probability for three-dimensional blades is 14 percent more than that for one-dimensional blades. This is a relatively small increment, and the mean probability calculated from the simpler model should be sufficiently accurate for many purposes.

8 Conclusions

A mathematical model that describes the dimensions and motions of birds and turbine blades can predict the probability of a collision when a model bird flies through the disk swept out by the rotor blades. The probability varies, depending on the point where the bird penetrates the disk. Along a given radius from the hub, the probabilities in most cases are higher near the rotor hub than at the periphery of the disk. At a given distance from the hub, probabilities are higher above and below the hub than to either side. For given wind conditions, the mean probability averaged over the surface of the disk is lower for downwind flight than for upwind or crosswind flight.

References

- Beyea, J., 1995, "Avian Issues in Wind Development." A presentation to the American Wind Energy Association by the Audubon Vice President for Science Policy, Washington, DC, Mar. 29, 1995.
- Davidson, R., 1994, "Bird Watching," *Windpower Monthly*, Vol. 10, No. 11, p. 18.
- Everett, G., 1993, "An Update of Wind Energy: After a Decade of Experiments, the Wind Industry is Finally Moving Inland," *Mother Earth News*, No. 137, No. 5, p. 78.
- Ferguson, R., 1993, "Birds and Wind Turbines: Can They Co-exist?" *CEERT Coalition Energy News*, Spring, pp. 9-10.
- Lamarre, L., 1992, "A Growth Market in Wind Power," *EPRI Journal*, Dec., 4-15.
- Manning, P. T., 1983, "The Environmental Impact of the Rise of Large Wind Turbines," *Wind Engineering*, Vol. 7, pp. 1-11.
- Spera, D. A., 1994, "Introduction to Modern Wind Turbines," *Wind Turbine Technology*, D. A. Spera, ed., ASME Press, New York, pp. 47-72.
- Tamkins, T., 1993, "Tilting at Wind Power: Wind is Clean and Efficient—and it can Kill Eagles," *Audubon*, Vol. 95, No. 3, p. 24.
- Tucker, V. A., 1996, "Using a Collision Model to Design Safer Wind Turbine Rotors for Birds," *ASME JOURNAL OF SOLAR ENERGY ENGINEERING*, Vol. 118, pp. 263-269.
- Wilson, R. E., 1994, "Aerodynamic Behavior of Wind Turbines," *Wind Turbine Technology*, D. A. Spera, ed., ASME Press, New York, pp. 215-282.
- Weinberg, C. J., and Ancona, D. F., 1994, "A Utility Perspective of Wind Energy," *Wind Turbine Technology*, D. A. Spera, ed., ASME Press, New York, pp. 589-602.
- Weisman, J., 1995, "Tilting at Windmills," *Wildlife Conservation*, Vol. 97, No. 1, pp. 52-57.
- Walcott, C., 1995, "Tilting at Windmills," *Living Bird*, Summer, pp. 10-15.

Using a Collision Model to Design Safer Wind Turbine Rotors for Birds

V. A. Tucker

Department of Zoology,
Duke University,
Durham, NC 27708

A mathematical model for collisions between birds and propeller-type turbine rotors identifies the variables that can be manipulated to reduce the probability that birds will collide with the rotor. This study defines a safety index—the "clearance power density"—that allows rotors of different sizes and designs to be compared in terms of the amount of wind energy converted to electrical energy per bird collision. The collision model accounts for variations in wind speed during the year and shows that for model rotors with simple, one-dimensional blades, the safety index increases in proportion to rotor diameter, and variable speed rotors have higher safety indexes than constant speed rotors. The safety index can also be increased by enlarging the region near the center of the rotor hub where the blades move slowly enough for birds to avoid them. Painting the blades to make them more visible might have this effect. Model rotors with practical designs can have safety indexes an order of magnitude higher than those for model rotors typical of the constant speed rotors in common use today. This finding suggests that redesigned rotors could have collision rates with birds perhaps an order of magnitude lower than today's rotors, with no reduction in the production of wind power. The empirical data that exist for collisions between raptors, such as hawks and eagles, and rotors are consistent with the model: the numbers of raptor carcasses found beneath large variable speed rotors, relative to the numbers found under small constant speed rotors, are in the proportions predicted by the collision model rather than in proportion to the areas swept by the rotor blades. However, uncontrolled variables associated with these data prevent a stronger claim of support for the model.

1 Introduction

Wind turbines generate electricity, but they also collide with birds. Development of wind power has stopped in some locations until some means of mitigating avian fatalities from collisions is found (Tucker, 1996). A mathematical model for collisions between birds and turbine rotors (Tucker, 1996) now offers the opportunity to design rotors that will mitigate collisions. The model identifies the variables that influence the probability of a collision when a bird flies through the area swept by the rotor blades, and some of these variables can be manipulated to make the turbine safer for birds.

This study uses the collision model to investigate the safety, in the context of bird collisions, of model turbine rotors of different designs with simple, one-dimensional blades. To do this, it first summarizes energy conversion by rotors, and then defines a safety index that depends on both the amount of electrical energy that a rotor produces, and the probability that the turbine rotor will collide with birds in the process. A model rotor designed for safety can have a safety index ten times higher than that of a model rotor with characteristics typical of rotors in use today. This finding suggests that a 90 percent mitigation of bird collisions could be achieved, with no reduction in the amount of electricity generated from the wind, by redesigning turbine rotors.

2 Characteristics of Model Turbines, Birds, and the Wind

Wind turbines have structural and aerodynamic characteristics described by Spera (1994) and Wilson (1994), and the

characteristics relevant to this study are mentioned here. The model turbine rotors are of the propeller type, mounted on horizontal shafts; and have B blades, where $B = 3$. A rotor rotates on the shaft at angular speed Ω and sweeps out a disk of radius R with surface area S :

$$S = \pi R^2. \quad (1)$$

For simplicity, the rotor blades are one dimensional with length being the only dimension; and a bird's flight path is always downwind and in the same direction as the wind. More complex analyses for three-dimensional blades and upwind and crosswind flight (Tucker, 1996) are beyond the scope of this study. Nevertheless, the general conclusions that can be drawn from the analysis of one-dimensional blades are plausible for three-dimensional blades, since both types have similar probabilities for colliding with birds. The mean probability of a collision during downwind flight through a rotor with three-dimensional blades was only 14 percent higher than for a comparable rotor with one-dimensional blades (Tucker, 1996), and this increment is small compared to the changes in some of the quantities discussed in this study.

A model bird is a two-dimensional object described in Tucker (1996). It has wing span b , aspect ratio A and air speed V_b .

Wind speed in nature usually changes from moment to moment, but if the wind speed averaged over a period of 0.1 hour does not change in successive periods, the wind speed is steady. This study refers to steady wind speeds that are horizontal in direction, constant in the region swept by the rotor blades and always parallel to the rotor shaft because the rotor yaws around a vertical axis when the wind direction changes.

Far upwind of the rotor disk, the wind has the speed U , but the wind transfers some of its kinetic energy to the rotor and slows down to speed $(1 - a)U$ as it moves through the rotor disk. The axial induction factor, a , changes in value from 0 far

Contributed by the Solar Energy Division of THE AMERICAN SOCIETY OF MECHANICAL ENGINEERS for publication in the ASME JOURNAL OF SOLAR ENERGY ENGINEERING. Manuscript received by the ASME Solar Energy Division, Sept. 1995; final revision, May 1996. Associate Technical Editor: P. S. Veers.

upwind of the disk to $\frac{1}{3}$ as the wind passes through a rotor that extracts a maximum proportion of energy from the air. This study uses a more realistic value 0.25 for a .

3 The Power and Power Density of the Wind

The power of the wind P_w is the rate at which moving air carries kinetic energy across a rotor disk of area S :

$$P_w = 0.5\rho SU^3, \quad (2)$$

where ρ is the density of the air (1.16 kg/m³ in this study).

The power density of the wind $P_{d,w}$ is the power per unit area of the rotor disk:

$$P_{d,w} = P_w/S = 0.5\rho U^3. \quad (3)$$

4 The Conversion of Wind Power to Electrical Power

The rotor produces electrical energy at rate P_o , the power output, by turning a generator. P_o is a fraction of P_w expressed by the power coefficient:

$$C_p = P_o/P_w. \quad (4)$$

The power coefficient has a theoretical maximum value of 0.59 (the Betz limit), and typical maximum values for actual rotors are near 0.4.

C_p can be found from data supplied by the turbine manufacturer, who usually reports P_o as a function of U . With Eq. (2), C_p becomes a function of U known as the characteristic curve for C_p . Since C_p is dimensionless, one characteristic curve can describe rotors of different sizes.

The power coefficient is functionally related to the tip speed ratio λ , given by

$$\lambda = \Omega R/U. \quad (5)$$

C_p has its maximum value $C_{p,0}$ when $\lambda = \lambda_0$, and λ_0 typically is between 5 and 8.

λ can be found from data supplied by the turbine manufacturer, who usually reports Ω as a function of U . With Eq. (5), λ becomes a function of U known as the characteristic curve for λ . Since λ is dimensionless, one characteristic curve can describe rotors of different sizes.

5 Special Wind Speeds

Certain wind speeds have special names because of the way that they affect rotors. A typical rotor remains stationary as the

wind speed increases from 0 to the *cut-in wind speed*. The rotor then begins to turn and produce electrical power. When the wind speed increases to the *design wind speed*, the rotor power coefficient is maximum. With a further increase to the *rated wind speed*, the rotor power output is maximum; and at higher wind speeds, control mechanisms keep the rotor power output maximum until wind speed reaches the *cut-out wind speed*. Then control mechanisms stop the rotor to protect it from wind damage.

6 Areas of the Rotor Disk

The *disk area* S has already been defined in Eq. (1).

The *active area* S_a is an area of the disk that the bird passes through without making any effort to avoid a blade (Tucker, 1996). S_a begins at radius r_0 from the center of the rotor and extends to R :

$$S_a = \pi(R^2 - r_0^2). \quad (6)$$

At r_0 , the blade has the tangential threshold speed v_0 , and at radii less than r_0 , the bird avoids the blades so that the probability of a collision is 0. This characteristic of the model bird is meant to represent the behavior of real birds, which are able to avoid collisions by flying around slow moving objects such as the rotor blades near the hub.

The behavior of real birds undoubtedly is more complex than a binary response to a threshold speed. The collision model (Tucker, 1996) includes a variable (p_a) that accounts for the actions that birds take action to avoid rotor blades, and v_0 provides a means of assigning a value of 0 or 1 to p_a . In fact, p_a probably is a continuous function of many variables—for example, the size, speed and orientation of the blade, its color and pattern, the background against which it is seen, the ambient light, the transparency of the air, the visual abilities of the bird, and whether the bird is intent on prey or a perch site. Unfortunately, not enough is known about bird behavior around turbines to construct a model of known accuracy for p_a , and the concept of a threshold velocity in this paper should be taken as a first approximation that allows numerical results to be calculated from the collision model.

In this study, v_0 is constant for a given rotor, and r_0 varies with Ω :

$$r_0 = v_0/\Omega. \quad (7)$$

Thus, S_a is constant for a constant speed (constant Ω) rotor, but changes with Ω for a variable speed rotor.

Nomenclature

A = aspect ratio of the bird
 a = axial induction factor
 B = number of blades in rotor
 b = wing span of the bird (m)
 C = Weibull scale factor (m/s)
 C_p = power coefficient
 $C_{p,0}$ = maximum power coefficient
 e = electrical energy produced from the wind per bird collision (J)
 f = frequency of annual wind speeds
 k = Weibull shape factor
 M_e = ratio of empirical collision rates
 M_S = ratio of collision rates proportional to disk area
 M_t = ratio of theoretical collision rates
 P_o = electrical power output of rotor (W)

\hat{P}_o = time-averaged power output (W)
 $P_{d,w}$ = power density of wind (W/m²)
 $P_{d,c}$ = clearance power density (W/m²)
 $\hat{P}_{d,c}$ = time-averaged clearance power density (W/m²)
 P_w = power of the wind (W)
 p = space-averaged probability of a collision
 p_a = probability of a collision due to active avoidance behavior
 Q = flow of birds through a unit of disk area in a unit of time (1/(m²s))
 R = maximum radius (m)
 r_0 = minimum radius (m)
 S = area of rotor disk (m²)
 S_a = active area of rotor disk (m²)
 S_c = clearance area of rotor disk (m²)
 \hat{S}_c = time-averaged clearance area (m²)

t = time (s or years)
 U = wind speed (m/s)
 U_0 = rated wind speed (m/s)
 U_i = cut-in wind speed
 U_o = cut-out wind speed
 V_b = bird speed relative to air (m/s)
 v_0 = tangential speed of blade at minimum radius (m/s)

Greek symbols

λ = tip-speed ratio
 λ_0 = tip-speed ratio at maximum power coefficient
 π = ratio of circumference to diameter of a circle
 ρ = density of air (kg/m³)
 Ω = angular speed of rotor (radians/s)
 Ω_0 = Ω for a constant speed rotor (radians/s)

The clearance area S_c is a quantity used in the calculation of the clearance power density in Section 8. S_c is a virtual area found by multiplying the active area by the probability p (see Section 7) that a collision will occur:

$$S_c = pS_a. \quad (8)$$

All birds flying through S_c must be "cleared" by collisions with the blades to account for the collision rate QpS_a , where Q is the number of birds passing through a unit area of the disk in a unit of time. (The term "clearance" comes from the field of renal physiology. The renal clearance of substance x is a virtual blood plasma flow rate, and the kidneys must clear (remove) all of substance x from this plasma flow to account for the rate at which they excrete x .)

7 The Probability That a Bird Will Collide With the Rotor, and the Clearance Area

The mean probability p that a model bird passing through the active area of the rotor disk will collide with a blade is given by Eq. (24) from Tucker (1996), where V_b is the downwind airspeed of the bird, and v_0/Ω is less than R :

$$p = \frac{Bb}{2\pi} \left(\frac{\Omega}{A|V_b + (1-a)U|} + \frac{4}{\pi \left(R + \frac{v_0}{\Omega} \right)} \right). \quad (9)$$

In this study, Ω , U , R , and v_0 may vary, and the remaining quantities on the right side of the equation are constant with the following values: B , the number of rotor blades, is 3; b , the wing span of the bird, is 1 m; A , the aspect ratio of the bird, is 2; V_b is 5 m/s and a , the axial induction factor, is 0.25. The wing span of the bird is typical of that of a Red-shouldered hawk (*Buteo lineatus*) or a small Red-tailed hawk (*Buteo jamaicensis*), and the air speed is typical of slow gliding.

An expression for the clearance area S_c now may be found by multiplying Eq. (9) by Eq. (6), replacing r_0 with v_0/Ω from Eq. (7), and replacing Ω with $\lambda U/r$ from Eq. (5). After rearrangement,

$$S_c = \frac{BbR}{2} \left(1 - \frac{v_0}{\lambda U} \right) \left(\frac{\lambda U + v_0}{A|V_b + (1-a)U|} + \frac{4}{\pi} \right). \quad (10)$$

If $v_0/(\lambda U)$ is greater than 1, S_c is 0.

Equation (10) shows that S_c is proportional to R when the other quantities on the right side of the equation are constant, and the mean value of S_c is also proportional to R in a regime of variable wind speeds to be described later.

8 A Safety Index: The Clearance Power Density

This section introduces a safety index for turbine rotors that takes into account both the electrical energy produced by the rotor and the probability of collisions with birds. Both factors need to be considered. For example, two rotors of different designs might collide with the same proportion of birds that passed through their disks in a year, but the rotor that produced a greater amount of electrical energy in the year should have a higher safety index. If the safety index neglected energy production and accounted for only the probability of a collision, use of the index to evaluate rotor designs would lead to rotors that collided with few birds but produced no electrical energy.

The safety index proposed here is a ratio of power to an area, and hence it is a power density. Specifically, it is the clearance power density, the ratio of the power output of the rotor to the clearance area:

$$P_{dc} = P_o/S_c. \quad (11)$$

From Eq. (8), the collision rate of birds with the rotor is QS_c ,

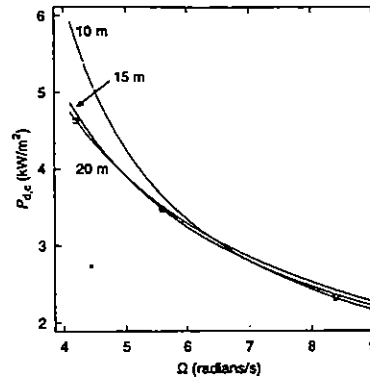


Fig. 1 Clearance power density, P_{dc} , at different angular speeds, Ω , for rotors with radii of 10, 15, and 20 m. The design wind speed is 12 m/s and the power coefficient is 0.4. Circles on each curve mark the combinations of radius and speed that give tip-speed ratios of seven.

and the electrical energy, e , produced from the wind per bird collision is

$$e = P_{dc}/Q. \quad (12)$$

e can be thought of as an inverse tax rate, since its reciprocal measures the cost in bird collisions to produce a unit of electricity. Safer rotors have higher values of e for a given Q .

The clearance power density could, in principle, be used to determine e , but unfortunately, Q usually is unknown and is difficult to measure. Even so, P_{dc} is useful for comparing the safety of rotors of different sizes, tip-speed ratios, and power coefficients when Q can be considered constant. Suppose rotors 1 and 2 had different designs, and both operated in the same locality at the same time so that wind conditions and Q were the same for both. Then Q cancels, and

$$e_1/e_2 = (P_{dc})_1/(P_{dc})_2, \quad (13)$$

where the subscripts indicate the rotor design. In this case, the ratio of the clearance power densities measures the relative safety for birds of the two rotor designs.

For example, suppose turbines with rotors of either design 1 or 2 could be installed in sufficient numbers at a windplant to produce a given amount of electrical energy per year. Both designs would be exposed to the same annual wind conditions and Q , and design 1 has a P_{dc} value three times that of design 2 for the annual wind conditions. The windplant operator, by choosing design 1 for its higher clearance power density, could reduce the number of bird strikes per year by $\frac{2}{3}$ with no reduction in electrical production.

9 Comparison of Different Model Rotor Designs

This section compares the clearance power densities of different rotor designs in two wind regimes. The first regime is simple: the wind speed remains constant at the design speed. In the second regime, the wind speed varies between the cut-in and cut-out speeds over the course of a year, and a mean clearance power density is computed from time-averaged power output and clearance area of the rotor.

9.1 Operation at the Design Wind Speed. The model rotors discussed here demonstrate the effect of only two variables on clearance power density P_{dc} : the angular speed Ω and the radius R of the rotor. All other quantities are constant: the wind speed is the design speed (12 m/s), the power coefficient is 0.4, v_0 is 25 m/s and the other quantities have the values given in the text that describes Eq. (9). The value of v_0 is unknown, but 25 m/s is a plausible estimate, judging from the behavior of real birds near moving automobiles.

Figure 1 shows curves that relate Ω and P_{dc} for rotor disks of three radii. Each combination of Ω and R on a curve deter-

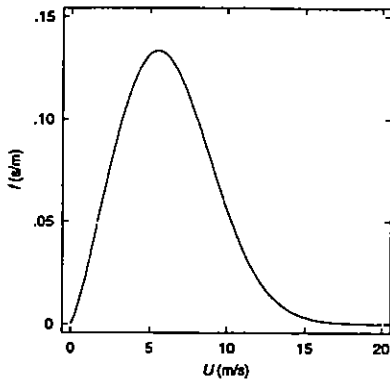


Fig. 2 The reference Weibull wind speed distribution function.

mines a tip speed ratio λ_0 at the design speed, and a circle on each curve marks the point for $\lambda_0 = 7$. Changes in R have little effect on P_{dc} when Ω is constant. However, rotors of all sizes must operate at λ_0 near seven to achieve high power coefficients, and when $\lambda_0 = 7$, the larger the rotor, the safer the turbine will be. For constant λ , P_{dc} is proportional to R , irrespective of the value of v_0 , since P_o is proportional to R^2 (Eqs. (2) and (4)) and S_c is proportional to R (Eq. (10)). Nor is the proportionality the result of a disproportionate increase in r_0 , since Eqs. (5) and (7) show that $r_0 = 0.3R$ for all of the rotors in Fig. 1.

9.2 Operation Between Cut-In and Cut-Out Wind Speeds. The previous section analyzed changes in P_{dc} at constant wind speed, and this section extends that analysis to wind speeds that change throughout the year. Wind speed influences both the power output and the clearance area of a rotor, and time-averaged values of these quantities define the mean P_{dc} for a year. The design of the model rotor markedly affects the mean P_{dc} .

9.2.1 The Frequency Distribution of Wind Speeds. The Weibull distribution is commonly used to describe the frequency distribution function of wind speeds over a year (Spera, 1994):

$$f = (k/C)(U/C)^{k-1} \exp[-(U/C)^k], \quad (14)$$

where f is the value of the frequency distribution function in fractions of a year per unit wind speed, and f has units of reciprocal m/s. For example, the number of hours per year that the wind blows at speeds between $U - 0.5$ and $U + 0.5$ m/s is $f \times 8760$ hours/year. The quantities C and k are scale and shape factors, respectively, that can be fitted to observed wind speed frequencies. For comparative purposes, designers use $C = 7.07$ m/s and $k = 2.29$ to define a reference Weibull wind speed distribution function (Fig. 2) (Frost and Aspliden, 1994), and this study uses this reference distribution.

9.2.2 The Mean Power Output, Clearance Area, and Clearance Power Density of the Rotor for a Year. The mean power output \bar{P}_o of the rotor during a year can be found for the reference Weibull wind speed distribution by integration:

$$\bar{P}_o = \frac{1}{t_1 - t_0} \int_{t_0}^{t_1} P_o dt = \int_{U_i}^{U_o} P_o f dU, \quad (15)$$

where $t_1 - t_0$ is one year, and U_i and U_o are the cut-in and cut-out wind speeds, respectively (see Frost and Aspliden, 1994, for the method of changing the variable of integration from t to U). The integration is ordinarily done numerically.

The mean clearance area during a year also can be found for the reference Weibull wind speed distribution by numerical integration:

$$\bar{S}_c = \int_{U_i}^{U_o} S_c f dU. \quad (16)$$

The mean clearance power density is

$$\bar{P}_{dc} = \bar{P}_o / \bar{S}_c. \quad (17)$$

9.2.3 Examples. As examples of mean clearance power densities for the reference Weibull wind speed distribution, this study describes model rotors of two sizes—one with a radius of 10 m, which is similar in size to many rotors now in use; and one with a radius of 20 m, which is similar in size to new rotors now in production. The cut-in and cut-out speeds are 5 and 20 m/s, v_0 is 25 m/s; and at the rated wind speed U_0 of 12 m/s, C_p has its maximum value $C_{p,0}$ of 0.4, and $\lambda_0 = 7$. The value of ΔU used for numerical integration is 1 m/s, and the text that describes Eq. (9) gives the values of other quantities. The rotors are of two types—constant speed and variable speed. The examples comprise all four combinations of size and type, and show how these characteristics affect the mean clearance power density.

9.2.3.1 Constant speed rotors. When wind speed reaches the cut-in speed, this type of rotor accelerates from a standstill to Ω_0 , a constant value that it maintains until the cut-out speed. Consequently, the tip speed ratio λ declines as wind speed increases, since

$$\lambda = \Omega_0 R / U. \quad (18)$$

Constant speed rotors have the virtue of turning an electrical generator at a constant speed and thereby generating alternating current at the same phase and frequency as that of the transmission lines. However, they have low power coefficients at low and high wind speeds where λ is above and below λ_0 , respectively.

The characteristic curve for C_p (Fig. 3) used in the examples increases from 0 at the cut-in speed to $C_{p,0} = 0.4$ at the rated wind speed U_0 , which is the same as the design speed. At higher wind speeds, C_p declines because the turbine controls keep power output constant:

$$C_p = C_{p,0} U_0^3 / U^3. \quad (19)$$

The characteristic curve for λ (Fig. 3) also declines with increasing U , since Ω is constant:

$$\lambda = \lambda_0 U_0 / U. \quad (20)$$

9.2.3.2 Variable speed rotors. At the cut-in speed, a typical variable speed rotor accelerates to the value of Ω for λ_0 . As wind speed increases, Ω increases to keep λ constant until

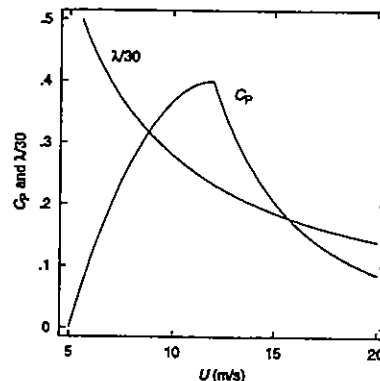


Fig. 3 Characteristic curves for the power coefficient, C_p , and the tip-speed ratio, λ , for constant-speed rotors as the wind speed, U , varies between cut-in and cut-out speeds. Between $U = 5$ and 12 m/s, $C_p = -0.776 + 0.1960 U - 0.00816 U^2$. The text gives equations for the other curves.

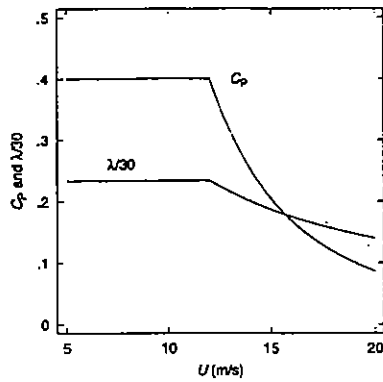


Fig. 4 Characteristic curves for the power coefficient, C_p , and the tip-speed ratio, λ , for variable speed rotors as the wind speed, U , varies between cut-in and cut-out speeds.

the wind speed reaches the rated wind speed. Then the turbine controls keep Ω and P_o constant, and λ and C_p decline.

Variable speed rotors have higher power coefficients than constant speed rotors at wind speeds between the cut-in speed and the rated speed, because $\lambda = \lambda_0$ over this range. However, a variable speed rotor cannot turn a directly connected generator at constant speed and requires another device to synchronize the generated current with the alternating current carried by the transmission lines.

The characteristic curves (Fig. 4) used in the examples show that $C_p = 0.4$ and $\lambda = 7$ up to the rated speed, at which point the power output and Ω become constant. Above the rated speed, C_p and λ are given by Eq. (19) and (20); and both variable and constant speed rotors have the same characteristic curves.

9.2.3.3 Turbine matrix. \hat{P}_{dc} varies for the four-model rotor designs by a factor of nearly five (Table 1). The small, constant-speed rotor has characteristics that are typical of most real rotors operating today and has the lowest \hat{P}_{dc} . Two factors keep \hat{P}_{dc} low: (1) the rotor produces little power during 60 percent of the year when wind speeds are above the cut-in speed but below the rated speed (Fig. 2). Power output is low because the power density of the wind is low, and C_p is low because λ is above λ_0 . (2) Even though the rotor produces little power at low wind speeds, it is dangerous to birds because it spins at the same rate between the cut-in wind speed and the rated speed. In fact, the rotor is more likely to collide with birds at the cut-in speed because at low wind speed, the bird has a low ground speed and takes a longer time to pass through the rotor disk.

The large, variable speed rotor has the highest \hat{P}_{dc} . For the model rotor designs in Table 1, a variable speed rotor of a given size is always less dangerous to birds than a constant speed rotor for two reasons: (1) the variable speed rotor harvests more wind energy between the cut-in wind speed and the rated speed because $\lambda = \lambda_0$ and C_p is maximum, and (2), the rotor spins more slowly at the cut-in speed than at the rated speed, and thus is less likely to collide with birds between these speeds.

Table 1 The mean clearance power density, \hat{P}_{dc} , for rotors of two types and sizes, in units of kW/m^2 . Numbers in parentheses are multiples of \hat{P}_{dc} , relative to the constant speed rotor with a radius of 10 m.

Rotor type	Rotor radius (m)	
	10	20
constant speed	0.442 (1.0)	0.885 (2.0)
variable speed	1.085 (2.5)	2.171 (4.9)

\hat{P}_{dc} is proportional to R for both the constant speed and variable speed rotors in Table 1. This proportionality arises because, for a given v_0 and wind speed distribution, Eqs. (2) and (4) show that \hat{P}_o is proportional to R^2 and Eq. (10) shows that \hat{S}_c is proportional to R . \hat{P}_{dc} is the ratio of these quantities (Eq. (17)).

The use of the threshold speed v_0 to describe bird behavior is not required for the proportional relation between \hat{P}_{dc} and R . v_0 determines the radius r_0 (Eq. (7)) of an area on the disk where no collisions occur, and this area changes on a variable speed rotor as Ω changes with wind speed. As an alternate model of bird behavior, r_0 can be set to a constant fraction of R , independent of wind speed or R . \hat{P}_{dc} is also proportional to R with this model.

10 Maximizing Clearance Power Density

The model rotors in Table 1 are typical of existing rotors that have been designed for high \hat{P}_o values, and the collision model shows how to design model rotors for high \hat{P}_{dc} values: The rotor should be variable speed and as large as possible. Multispeed rotors, e.g., those with a high and a low constant speed, will be safer than single speed rotors. The tip-speed ratio should be as low as possible without penalizing the power coefficient excessively. The threshold tangential speed v_0 should be as large as possible. (v_0 presumably could be increased by painting the blades to make them more visible, and this presumption can be tested experimentally.)

Figure 5 describes model constant and variable speed rotors, and some of the latter have combinations of R , λ_0 and v_0 that produce high \hat{P}_{dc} values. The characteristic curve for C_p for the variable speed rotors is that in Fig. 4, but the characteristic curve for λ depends on λ_0 : $\lambda = \lambda_0$ for wind speed between cut-in speed and the rated wind speed U_0 (12 m/s). Above U_0 , Eq. (20) gives λ . Other quantities have the values used for the previous examples.

Figure 5 shows that \hat{P}_{dc} values can be greatly increased above those for model rotors with characteristics typical of most rotors operating today. The most commonly used rotors turn at constant speed and have radii near 10 m. A model constant speed rotor of this size has a \hat{P}_{dc} value less than 0.5 kW/m^2 , and this value can be increased 2.5-fold solely by making the rotor variable speed. \hat{P}_{dc} is markedly dependent on v_0 . A \hat{P}_{dc} value of 10 kW/m^2 might be achieved with other changes, and this value could serve as a practical design goal for real rotors, which may have a power coefficient above 0.4 at a tip-speed ratio of five (Shimuzu et al., 1995).

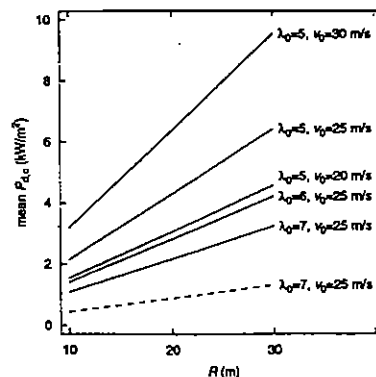


Fig. 5 Mean clearance power densities, \hat{P}_{dc} , for variable speed rotors (solid lines) and constant speed rotors (dashed line) with different radii, R , and various values of λ_0 and v_0 . All rotors operate in the reference Weibull distribution of wind speeds between cut-in and cut-out speeds of 5 and 20 m/s. See text for the values of other quantities.

11 Using the Collision Model to Design Real Rotors

The collision model can be useful in evaluating the safety of real rotors, even though parts of the model are untested. These parts are plausible and testable, although measurements are difficult to make on birds that move at their own volition through three-dimensional space. The greatest difficulty is the rarity of collisions between birds and rotors. Over a four-year period, searchers found only 0.03 raptor carcasses per turbine year beneath turbines at the Altamont Pass, CA (Howell, 1995). At this rate, one could expect to watch a turbine for 33 years on average before seeing a collision. Unless the flow rate of birds through a rotor can be experimentally augmented, avian experimentation takes too long to be useful.

The model suggests that a practical rotor can be designed with a safety index several times higher than those of typical constant speed rotors, and that the new rotor could produce more electrical energy each year while colliding with fewer birds. Given that there is an immediate need to reduce avian fatalities caused by rotors, that increased energy production theoretically can subsidize the costs of making rotors safer, and that the research needed to test the model thoroughly will take years; using the model now to evaluate the safety of rotors seems like a prudent decision.

Actual turbines designed for bird safety need not be copies of the model rotors described in this paper. For example, both variable and constant speed model rotors had the same cut-in speed, but actual variable speed rotors can have lower cut-in speeds to take advantage of their higher power coefficients at low wind speeds. This change reduces the disparity in safety indices; but not much, because a variable speed rotor turns too slowly at its cut-in speed to have a high probability of striking birds.

The location of a turbine also should be considered. The flow rate of birds (Q) and the wind speed obviously vary in time and space (including in different regions of the rotor disk); and a rotor with a high safety index, but located where Q is high, might still collide with an unacceptable number of birds per unit of electrical energy produced. The annual wind speed distribution at a location may not be the reference distribution used for the model rotors, and the wind speed distribution influences the safety index.

Finally, the design of turbine parts other than the rotor may influence bird safety. For example, the turbine tower and nacelle may offer perching sites that increase Q by attracting birds, and the design of these parts should be evaluated accordingly.

12 An Empirical Test of the Collision Model

The predictions of the collision model can be tested by counting the number of collisions that occur during an integral number of years while Q birds pass through the rotor disk per unit time per unit area of the disk. Q need not be known to compute the ratio of the collision rates at two different turbine types with the same Q . From Eq. (8) and (16), the ratio of the collision rates at turbine type 1 and turbine type 2 under these conditions is

$$M = \hat{S}_{c,1}Q/(\hat{S}_{c,2}Q) = \hat{S}_{c,1}/\hat{S}_{c,2}. \quad (21)$$

The following discussion uses M_i to denote a theoretical value computed from the collision model, and M_e to denote an empirical value computed from the number of bird carcasses collected under the two types of turbines, assuming that the number of carcasses is proportional to the number of collisions.

Howell (1995) investigated the avian collision rates at two types of turbines by collecting bird carcasses at two wind plants in California: Altamont Pass and the Montezuma Hills. Turbine type 1 was a Kenetech Corporation KVS-33 variable speed machine with a rotor radius of 16.5 m and a characteristic curve for λ shown in Fig. 4. Turbine type 2 was a Kenetech

Corporation KCS-56 constant-speed machine ($\Omega_0 = 7.54$ radians/s) with a rotor radius of 8.99 m and a characteristic curve for λ given by Eq. (18). At each wind plant, Howell collected under both types of turbine and selected turbines that were located in similar habitat.

For the computation of M_i , the rotors were assumed to operate in the reference Weibull wind speed distribution, to have cut-in and cut-out speeds of 5 and 20 m/s, and to have a tangential threshold speed v_0 of 25 m/s. Other quantities had the values given for Eq. (9). Then,

$$M_i = 1.24. \quad (22)$$

The empirical ratio, M_e , of collision rates is

$$M_e = 1.37, \quad (23)$$

calculated from 15 carcasses found under 53 KVS-33 turbines and 39 carcasses found under 188 KCS-56 turbines monitored for ten months (Montezuma Hills) or 18 months (Altamont Pass) (Howell, 1995). M_e is a weighted average that accounts for the differences in numbers of turbines and monitoring periods.

The empirical data are consistent with the collision model, but there are too many uncontrolled variables and too few data to make a strong claim that the data support the model. The assumptions of the reference wind speed distribution and equal cut-in and cut-out speeds for the two types of turbines introduce errors, and so may the assumption of equal Q values. The monitored turbines may have differed in ways that had unknown effects on Q : location, local abundance of prey, height of the rotor disk above the ground and whether the turbine tower and nacelle offered attractive perches to birds. Different proportions of birds may have passed through the rotors in downwind, upwind and crosswind directions. Now that the collision model has identified these variables, future studies of bird mortality can be designed to measure some of them.

Perhaps it seems paradoxical that the larger, variable speed KVS-33 collides with more birds than the KCS-100 in a given time ($M_i = 1.24$), yet is a safer turbine ($\hat{P}_{d,c} = 1.8$ for the KVS-33 versus $\hat{P}_{d,c} = 0.5$ for the KCS-100, assuming the C_p values shown in Figs. 3 and 4). The explanation is that $\hat{P}_{d,c}$ accounts for energy production as well as collisions, and the KVS-33 produces 4.4 times as much energy as the KCS-100.

Another model for predicting the ratio of collision rates at turbines of different types proposes that turbines kill birds in proportion to their disk areas S (Howell (1995). See also Tamkins, 1993; Weisman, 1994). The collision ratio, M_s , for this model is

$$M_s = S_1Q_1/(S_2Q_2). \quad (24)$$

When $Q_1 = Q_2$, M_s for the KVS-33 and the KCS-56 turbines is

$$M_s = (16.5/8.99)^2 = 3.37, \quad (25)$$

which is at least 2.5 times larger than M_i or M_e . Neither the collision model nor empirical data are consistent with the hypothesis that the collision rate is proportional to the disk area of a turbine.

13 Conclusions

A bird that flies through a turbine rotor has some probability of colliding with the rotor blades, and a mathematical model for collisions between birds and one-dimensional rotor blades identifies the rotor characteristics that influence this probability. The characteristics of a model rotor can be chosen to give the rotor a high safety index—a quantity that measures, for a unit flow rate of birds through the rotor, the amount of electrical energy generated from the wind per bird collision.

The safety index depends on the dimensions and motions of both the rotor blades and the bird, as well as on the annual distribution of wind speeds that flow through the rotor. A model rotor designed for a high safety index is variable speed, has a large diameter, a low tip-speed ratio and a large region near the rotor hub where the blades move slower than a threshold speed, below which birds can avoid the blades. Presumably, the threshold speed can be increased by painting the blades to make them more visible. This rotor may have a safety index an order of magnitude higher than that of a model constant speed rotor with characteristics typical of most rotors in use today. These findings for model rotors suggest that real rotors could be redesigned to greatly reduce the rate of bird collisions, with no reduction in electrical energy generated each year.

The field data that are available to test the collision model are consistent with the findings for model rotors described above. The numbers of raptor carcasses collected beneath large, variable speed rotors, relative to those collected beneath small constant speed rotors, are as predicted by the model; and are not proportional to the relative areas of the rotor disks. However,

these findings are not a rigorous test of the model because of uncontrolled variables.

References

Frost, W., and Aspliden, C., 1994, "Characteristics of the Wind," *Wind Turbine Technology*, D. A. Spera, ed., ASME Press, New York, pp. 371-445.

Howell, J. A., 1995, "Avian Mortality at Rotor Swept Area Equivalents, Altamont Pass and Montezuma Hills, California," A Report to Kenetech Windpower from Judd Howell & Associates, 3030 Bridgeway, Suite 119, Sausalito, CA 94965.

Shimizu, Y., Imamura, H., Matsumura, S., Maeda, T., and van Bussel, G. J. W., 1995, "Power Augmentation of a Horizontal Axis Wind Turbine Using a Mie Type Tip Vane: Velocity Distribution Around the Tip of a HAWT Blade With and Without a Mie Type Tip Vane," *ASME JOURNAL OF SOLAR ENERGY ENGINEERING*, Vol. 117, pp. 297-303.

Spera, D. A., 1994, "Introduction to Modern Wind Turbines," *Wind Turbine Technology*, D. A. Spera, ed., ASME Press, New York, pp. 47-72.

Tamkins, T., 1993, "Tilting at Wind Power: Wind is Clean and Efficient—and It Can Kill Eagles," *Audubon*, Vol. 95, No. 3, p. 24.

Tucker, V. A., 1996, "A Mathematical Model of Bird Collisions with Wind Turbine Rotors," *ASME JOURNAL OF SOLAR ENERGY ENGINEERING*, Vol. 118, pp. 253-262.

Wilson, R. E., 1994, "Aerodynamic Behavior of Wind Turbines," *Wind Turbine Technology*, D. A. Spera, ed., ASME Press, New York, pp. 215-282.

Weisman, J., 1995, "Tilting at Windmills," *Wildlife Conservation*, Vol. 97, No. 1, pp. 52-57.

<p>If you are planning To Move, Please Notify The ASME-Order Dep't 22 Law Drive Box 2300 Fairfield, N.J. 07007-2300</p> <p>Don't Wait! Don't Miss An Issue! Allow Ample Time To Effect Change.</p>	<p style="text-align: center;">Change of Address Form for the Journal of Solar Energy Engineering</p> <p style="text-align: center;">Present Address - Affix Label or Copy Information from Label</p> <div style="border: 1px solid black; height: 60px; margin: 10px auto; width: 80%;"></div> <p style="text-align: center;">Print New Address Below</p> <div style="border: 1px solid black; padding: 5px; margin-top: 10px;"> <p>Name _____</p> <p>Attention _____</p> <p>Address _____</p> <p>City _____ State or Country _____ Zip _____</p> </div>
--	--